



Biomechanical evaluation of flash-frozen and cryo-sectioned papillary muscle samples by using sinusoidal analysis: cross-bridge kinetics and the effect of partial Ca^{2+} activation

Jing Xi^{1,4} · Han-Zhong Feng² · Jian-Ping Jin² · Jinxiang Yuan³ · Masataka Kawai⁴

Received: 30 October 2023 / Accepted: 8 February 2024 / Published online: 16 April 2024
© The Author(s), under exclusive licence to Springer Nature Switzerland AG 2024

Abstract

We examined the integrity of flash-frozen and cryo-sectioned cardiac muscle preparations (introduced by Feng and Jin, 2020) by assessing tension transients in response to sinusoidal length changes at varying frequencies (1–100 Hz) at 25 °C. Using 70- μm -thick sections, we isolated fiber preparations to study cross-bridge (CB) kinetics: preparations were activated by saturating Ca^{2+} as well as varying concentrations of ATP and phosphate (Pi). Our results showed that, compared to ordinary skinned fibers, in-series stiffness decreased to 1/2, which resulted in a decrease of isometric tension to 62%, but CB kinetics and Ca^{2+} sensitivity were little affected. The pCa study demonstrated that the rate constant of the force generation step ($2\pi b$) is proportionate to $[\text{Ca}^{2+}]$ at $< 5 \mu\text{M}$, suggesting that the activation mechanism can be described by a simple second order reaction. We also found that tension, stiffness, and magnitude parameters are related to $[\text{Ca}^{2+}]$ by the Hill equation, with a cooperativity coefficient of 4–5, which is consistent with the fact that Ca^{2+} activation mechanisms involve cooperative multimolecular interactions. Our results support the long-held hypothesis that Process C (Phase 2) represents the CB detachment step, and Process B (Phase 3) represents the force generation step. Moreover, we discovered that constant H may represent the work-performing step in cardiac preparations. Our experiments demonstrate excellent CB kinetics with two well-defined exponentials that can be more distinguished than those found using ordinary skinned fibers. Flash-frozen and cryo-sectioned preparations are especially suitable for multi-institutional collaborations nationally and internationally because of their ease of transportation.

Keywords Flash-frozen muscle preparation · Cryo-sectioned papillary muscle · Tension · Stiffness · Phosphate · ATP · Ca^{2+}

Abbreviations

A	Actin	ATP	Adenosine-5'-triphosphate, exists as MgATP^{2-} in myocytes
A	Magnitude of process A	B	Magnitude of Process B
Ac	Acetate	b	Characteristic frequency of Process B. $2\pi b$ is its apparent (= measured) rate constant.
ADP	Adenosine-5'-diphosphate, exists as $\text{MgADP}^{1.5-}$ in myocytes	C	Magnitude of Process C
AM	Actomyosin; actin and myosin		

✉ Masataka Kawai
masataka-kawai@uiowa.edu

Jing Xi
jingxisuda@163.com

Han-Zhong Feng
hzhfeng@uic.edu

Jian-Ping Jin
jppjin@uic.edu

Jinxiang Yuan
yuanjinxiang18@163.com

¹ School of Nursing, and Medical Skill Experiment Teaching Center, Suzhou Medical College, Soochow University, Suzhou 215006, China

² Department of Physiology and Biophysics, University of Illinois at Chicago, 835 S Wolcott Ave, Chicago, IL 60612, USA

³ The Collaborative Innovation Center, Jining Medical University, Jining 272067, China

⁴ Department of Anatomy and Cell Biology, College of Medicine, University of Iowa, Iowa City, IA 52242, USA

c	Characteristic frequency of Process C. $2\pi c$ is its apparent rate constant.	σ	See Eq. 6 for definition
Ca_{50}	Apparent Ca dissociation constant, based on pCa-tension plot	S_{act}	Ca activatable stiffness
Ca_{50Y}	Apparent Ca dissociation constant, based on pCa-stiffness plot	S_{LC}	Low Ca^{2+} stiffness
CB	Cross-bridge	Stiffness	Young's elastic modulus (unit: Pascal or Pa) extrapolated to the infinite frequency (Y_{∞})
CK	Creatine kinase	T_{act}	Ca activatable tension
CM	Complex modulus	T_{LC}	Low Ca^{2+} tension
CP	Creatine phosphate, phosphocreatine	VM	Viscous modulus = $Imag [Y(f)]$
D	ADP, or MgADP	X_0	Probability of CBs in the AM.ADP state
D	= $[MgADP]$, concentration of $\frac{MgADP}{\sqrt{EM^2 + VM^2}}$	X_1	Probability of CBs in the AM state
DM	Dynamic modulus = $ Y(f) = \sqrt{EM^2 + VM^2}$	X_2	Probability of CBs in the AM.ATP state
ECM	Extracellular matrix	X_{012}	Probability of strongly attached CBs after work performance. $X_{012} = X_0 + X_1 + X_2$
EGTA	Ethylene glycol-bis(β -aminoethyl ether)-N,N,N',N'-tetraacetic acid	X_{34}	Probability of CBs in the detached and weakly attached states
EM	(Young's) elastic modulus = $Real [Y(f)]$	X_5	Probability of CBs in the AM*ADP.Pi state
f	Frequency used for sinusoidal analysis	X_6	Probability of CBs in the AM*ADP state
H	Complex modulus at $f \rightarrow 0$, and may include Process A in cardiac preparations	X_{56}	Probability of CBs after force generation, but before work performance, $X_{56} = X_5 + X_6$
i	$i = \sqrt{-1}$, Imaginary number	X_{01256}	Probability of CBs in the strongly attached states. $X_{01256} = X_0 + X_1 + X_2 + X_5 + X_6 = 1 - X_{34}$
K_0	CB's MgADP association constant	Y_{∞}	Young's elastic modulus extrapolated to the infinite frequency ($f \rightarrow \infty$). This property is called "stiffness" in this paper
K_1	CB's MgATP association constant	Y_{obs}	Observed complex modulus
K_2	The equilibrium constant of CB detachment Step 2	$Y(f)$	Complex modulus
K_4	The equilibrium constant of force generation Step 4	Y_{act}	Ca activatable stiffness
K_5	CB's phosphate (Pi) association constant. $1/K_5$ is Pi dissociation constant	Y_{LC}	Low Ca^{2+} stiffness
L_0	Length of muscle preparation		
n_H	Cooperativity (Hill coefficient) measured from pCa-tension plot		
n_{HY}	Cooperativity (Hill coefficient) measured from pCa-stiffness plot		
P	$P = [Pi] = [\text{phosphate}]$, phosphate concentration		
π	Circumference ratio, $\pi = 3.14159265 \dots$		
pCa	= $-\text{Log}_{10}[Ca^{2+}]$		
pCa ₅₀	= $-\text{Log}_{10}[Ca_{50}]$, calcium sensitivity measured from pCa-tension curve		
pCa _{50Y}	= $-\text{Log}_{10}[Ca_{50Y}]$, calcium sensitivity measured from pCa-stiffness curve		
pH	= $-\text{Log}_{10}[H^+]$		
PH	Phase shift = $\arg [Y(f)]$		
Pi	Phosphate		
r_2	Rate constant of CB detachment Step 2		
r_{-2}	Rate constant of CB's reverse detachment Step 2		
r_4	Rate constant of force generation Step 4		
r_{-4}	Rate constant of reverse force generation Step 4		
r_6	Rate constant of work performing Step 6		
S	ATP, or MgATP (substrate for actomyosin ATPase)		
S	Substrate concentration, $S = [MgATP]$		

Introduction

The exploration of active muscle mechanics and kinetics has evolved over time as simpler preparations were introduced to unravel the intricate workings of muscle function. Early investigations employed intact muscles (Hill 1938, 1953; Podolsky 1960) and intact single muscle fibers (Gordon et al. 1966) that were activated by electrical stimulation. Subsequently, glycerinated fibers (Ruegg and Tregear 1966; Pringle 1967) and skinned fibers (Hellam and Podolsky 1969; Reuben et al. 1971) were introduced, followed by split fibers (Sugi and Gomi 1984). More recently, researchers have focused on studying single myofibrils (Bartoo et al. 1993; Colomo et al. 1997; Tesi et al. 2000; Stehle et al. 2002; Rassier et al. 2003). Skinned fiber-to-myofibril preparations offer many advantages for investigating muscle mechanics and kinetics. They allow for the perfusion of experimental chemicals, such as Ca^{2+} , ATP, ADP, and phosphate (Pi), directly to the cross-bridges (CBs) within the myofilament space, thus allowing more hypotheses to be tested than with intact fibers or with whole-muscle preparations. By maintaining high physiological concentrations of contractile proteins in these structured systems, the preparations

preserve the allosteric interactions (cooperativity) among participating macromolecules. In addition, experiments can be performed in physiological ionic strength solutions.

In contrast to the structured system, experiments on simplified systems have been carried out, such as solution studies of extracted and reconstituted contractile proteins, and more recently, the use of single molecule studies with *in vitro* motility assays. These techniques have had enormous impacts on muscle research. However, the results produced by these systems are not complete and are sometimes inaccurate because of diminished cooperative interactions between macromolecules and because experiments are performed in extremely low ionic strength solutions.

Recently, a technique involving flash-frozen and cryo-sectioned cardiac muscle preparation has been introduced by Feng and Jin (2020). In this report, our objective is to comprehensively assess the functional integrity of this preparation by using small amplitude sinusoidal length changes and analyzing concomitant amplitude and phase shift (or elastic and viscous moduli) of the force responses, called “force transients”, under a range of experimental conditions. The ability to easily transport and exchange samples prepared using this technique promises to promote collaborative research in laboratories at different institutions internationally, and to advance our understanding of muscle biomechanics.

Methods

Flash freezing of papillary muscles, and cryo-sectioning

These procedures were described in Feng and Jin (2020). In brief, adult C57BL/6 J mice were anesthetized with isoflurane, the heart was removed, and left ventricular papillary muscles (size: approximately 1 mm diameter \times 5 mm length) were isolated and flash frozen in liquid nitrogen. Since the preparations were small, the freezing was instantaneous, and no foreign chemicals were used in this process. The muscles were then placed in a 1.7-mL Eppendorff tube for storage at -80°C . Using a cryostat set at -20°C , each frozen papillary muscle was sectioned at a thickness of $70\ \mu\text{m}$ and a width of $120\text{--}140\ \mu\text{m}$. These muscle strips were then transferred to a 1.7-mL Eppendorff tubes containing a relaxation solution that consisted of 50% glycerol maintained at -20°C . The tube was shipped from University of Illinois at Chicago to University of Iowa in Iowa City with ice packs and kept in a -20°C freezer until used for biomechanical experiments. The microscopic images of the preparation is shown in Fig. 1.

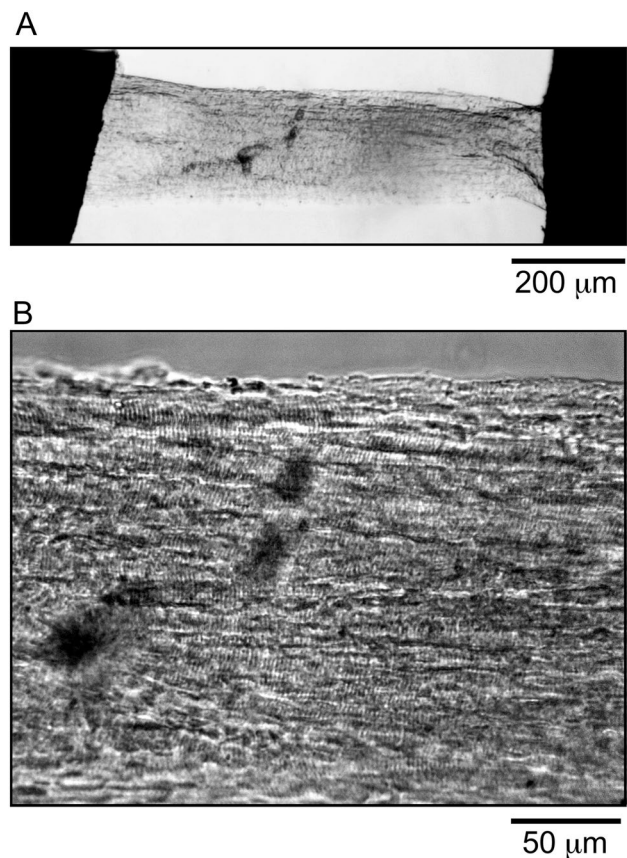


Fig. 1 Mouse cardiac muscle cryosections. Mouse left ventricular papillary muscle was cryo-sectioned into $70\text{-}\mu\text{m}$ -thick, $120\text{--}140\ \mu\text{m}$ wide strips. The strips were submerged in relaxing solution containing 50% glycerol at -20°C overnight before being skinned at 0°C in relaxing solution containing 1% triton X-100. The skinned strips were selected under a dissection microscope for containing longitudinally aligned cardiomyocytes. **A.** A strip mounted to force transducer with T-clips. **B.** The higher magnification bright field light microscopic image shows clear sarcomeric striations

Biomechanical experiments

On the day of experiments, a small bundle of the flash-frozen and cryo-sectioned preparation was further dissected from stored Sect. ($120\text{--}140\ \mu\text{m}$ wide and $70\ \mu\text{m}$ thick strips) to result in the width of $50\text{--}100\ \mu\text{m}$, the thickness of $70\ \mu\text{m}$, and the length of $1\text{--}2\ \text{mm}$, as measured under a dissecting microscope. This preparation was then carefully mounted in the experimental apparatus. One end of the bundle was connected to a linear motor (length driver) and the other end to a tension transducer via stainless steel wires, with a minute amount of nail polish. The bundles were then stretched until resting tension was just visible, resulting in a sarcomere length of $2.1\text{--}2.2\ \mu\text{m}$ as determined by optical diffraction at longer sarcomere lengths between 2.5 and $4.0\ \mu\text{m}$ (Wang et al. 2013a). However, the sarcomere length measurements had to be carried out in a separate preparation, because once

sarcomeres are stretched to these long lengths in a cardiac preparation, it becomes damaged and not suitable for the biomechanical studies. Isometric tension was recorded during full Ca^{2+} activation, which was then followed by the ATP study, the phosphate (Pi) study, the Ca^{2+} study, and the rigor study. When tension reached a steady value, sinusoidal analyses were performed with a range of 1–100 Hz (13 frequencies) at 0.2% amplitude. To test reproducibility, standard activation was repeated after each set of experiment (ATP study, Pi study, Ca^{2+} study); if tension reproducibility was < 90%, the data were excluded from analysis.

Sinusoidal analysis

This was carried out as described (Kawai and Brandt 1980; Kawai et al. 2021), and the complex modulus $Y_{\text{obs}} = Y(f)$ was obtained, which consists of a complex number, hence the name. The complex modulus contains two components: elastic modulus ($EM = \text{Real } Y(f)$), also called Young's elastic modulus) and viscous modulus ($VM = \text{Imag } Y(f)$). The complex modulus can also be expressed in the polar coordinates with dynamic modulus ($DM = |Y(f)| = \sqrt{EM^2 + VM^2}$) and phase shift ($PH = \text{arg } Y(f)$). The frequency-dependent complex modulus data were fitted to Eq. 1, which consists of two exponential Processes B and C in cardiac fibers (Kawai et al. 1993; Wannenburg et al. 2000) [see also (Shibata et al. 1987)] using a program developed in our laboratory, Dfit4.exe. The purpose of this fitting is to deduce the rate constants $2\pi b$ and $2\pi c$ of the exponential Processes B and C, respectively, in the most rational way.

$$Y(f) = H - \frac{Bfi}{b + fi} + \frac{Cfi}{c + fi} \quad (1)$$

where $i = \sqrt{-1}$. b is the characteristic frequency of exponential Process B, where B is its magnitude (strength; amplitude); c is the characteristic frequency of exponential Process C, where C is its magnitude; and H is a constant. From this point forward we will also refer to H as a magnitude parameter in cardiac preparations, for a reason that becomes apparent later. Processes B and C are called exponential processes because their time (t) domain expression $\Delta T(t)$ consists of exponential functions (Kawai and Brandt 1980):

$$\Delta T(t) = [H - B \exp(-2\pi bt) + C \exp(-2\pi ct)] \Delta L \quad (2)$$

where ΔL is the step length change, and $\Delta T(t)$ is the tension transient (time course). The algorithm to find b and c , as well as magnitude parameters H , B , and C from $Y(f)$ by data fitting with the program Dfit4.exe has been described (Kawai and Brandt 1980). In brief, these fitting parameters

are found to minimize $\sum |Y_{\text{obs}} - Y_{\text{theo}}|^2$, where the summation is over the frequencies used, and the theoretical projection Y_{theo} is calculated based on Eq. 1 at each frequency used for experiments. Y_{obs} is observed data point. The Young's elastic modulus extrapolated to the infinite frequency ($f \rightarrow \infty$) is defined by:

$$Y_{\infty} = Y(\infty) = H - B + C = EM(\infty) = DM(\infty) \quad (3)$$

In this report, this quantity is called "stiffness." Note that $VM(\infty) = 0$, therefore, all variables in Eq. 3 are real numbers. To normalize available data, magnitudes and related parameters are divided by Y_{∞} of the nearest standard activation (pCa 4.55, 5 mM MgATP, 8 mM Pi, 200 mM ionic strength). Thus, the unit of H , B , and C is Y_{∞} .

Y_{∞} corresponds to Phase 1 of step analysis, Process C to Phase 2, and Process B to Phase 3 (compare Eqs. 1 and 2). Step analysis also has been used to study CB kinetics (Huxley and Simmons 1971; Heinel et al. 1974; Huxley 1974; Ford et al. 1977). Process A has not been observed in cardiac muscles with experiments at ≤ 25 °C (Eqs. 1 and 2) (Kawai et al. 1993; Wannenburg et al. 2000), but it emerges with experiments at ≥ 30 °C (Lu et al. 2006). When characteristic frequencies are multiplied by 2π , these are called "apparent rate constants," signifying experimentally observed rate constants of exponential processes (see Eq. 2). These are equivalent to the rate constants deduced from tension transients of step analyses (Eq. 2), but not quite the same as the "intrinsic rate constants" or "fundamental rate constants" (Gutfreund 1995) of the elementary steps used to describe a CB model.

Standard activation and the rigor study

This was performed as shown in Fig. 2A. The fiber was first relaxed (R), followed by standard activation (A). Tension was increased to reach a plateau. After quickly carrying out sinusoidal analysis (0.4 s/frequency) at a low amplitude (0.2% L_0), the fiber was transferred to the rigor solution (Rig). Tension was further increased, followed by a decrease, taking several minutes to approach the steady state. Two to three sinusoidal analysis records were taken with a longer duration (1.6 s/frequency) and at an increased amplitude (0.35% L_0) to obtain data with a better signal-to-noise ratio (S/N). This was done because the rigor data were used to correct other experimental data for system response, most of which is caused by the tension transducer as described earlier (Kawai and Brandt 1980). In addition, fiber rundown is minimal with the rigor state compared to the Ca^{2+} -activated state(s), hence the quality of the preparation is maintained even after prolonging the data collection period and increasing the oscillation amplitude during rigor. In contrast, fiber

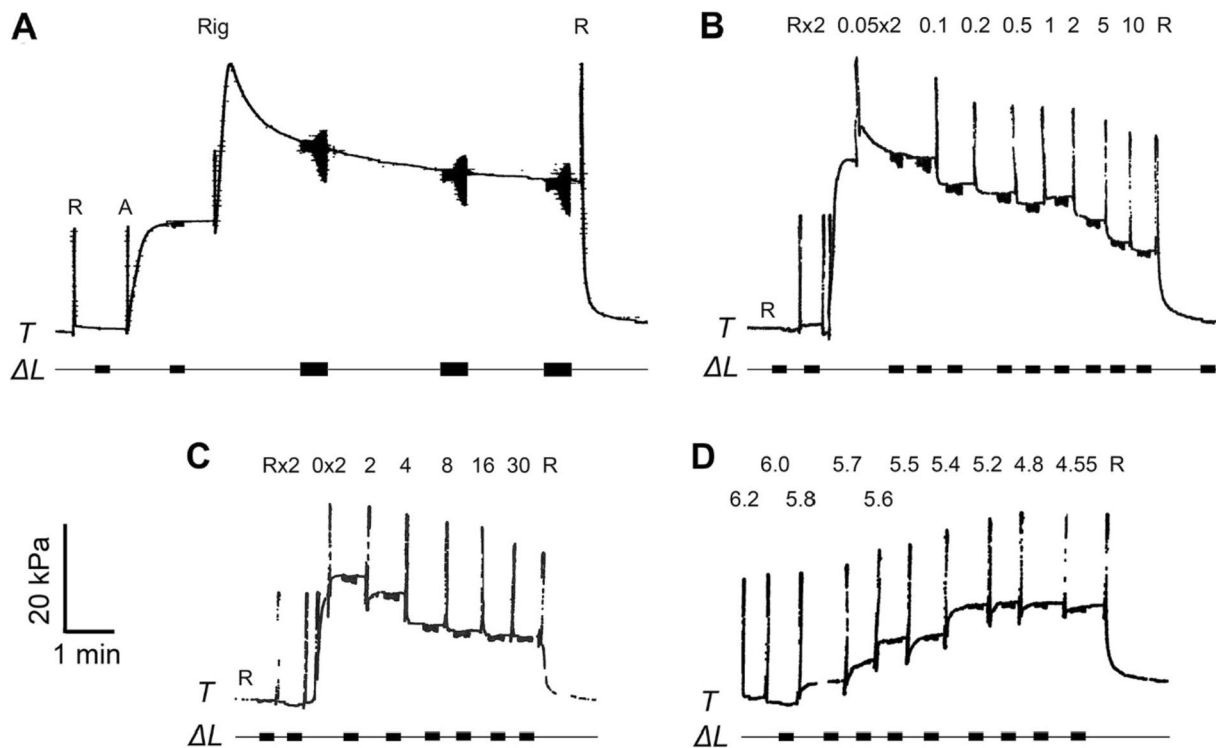


Fig. 2 Time course of tension (T) records in slow pen traces. **A** Standard activation and rigor study. R=Relaxing solution, A=standard activating solution, Rig=Rigor solution. **B** ATP study. The numbers indicate $[MgATP]$ in mM. **C**. Phosphate (Pi) study. The numbers indicate $[Pi]_{total}$ in mM. **D** Ca study. The numbers indicate pCa values. For **B** and **C** $\times 2$ indicates that the solution was changed twice. In all panels, the computer record of the length change (ΔL) is shown

below the tension time course. Amplitude was $0.2\% L_0$ (peak-to-peak was $0.4\% L_0$) for most experiments, except for the rigor condition (amplitude $0.35\% L_0$). For the rigor condition, the measurement duration was prolonged. The tension signal was filtered by a 10-Hz second order low-pass filter. Sharp vertical spikes indicate solution change artifacts. Scale bars represent 20 kPa (ordinate) and 1 min (abscissa)

rundown is faster when the fiber is activated with Ca^{2+} in the presence of ATP. This part of the experiments was usually carried out after the ATP and Pi studies. Rundown of the flash-frozen and cryo-sectioned preparations was not any different from ordinary fiber preparations.

ATP study and analysis of the apparent rate constant $2\pi c$

The ATP study was carried out as in Fig. 2B for the slow pen trace of the tension time course. Fibers were initially relaxed in relaxing solution (R), and then the solution was replaced twice with a solution that contained 0.05 mM MgATP in the presence of Ca^{2+} ($[Ca^{2+}] > 20 \mu M$). Because R contained 2 mM MgATP, the first solution change was used to wash out excess MgATP. Tension quickly developed to reach a plateau. The fiber length was then oscillated in a series of sine waves ranging between 1–100 Hz. Time course data from both the length (ΔL) and the force (ΔF) changes were collected every 10 μs , the signal was averaged on each sinusoidal cycle, and the complex modulus data $Y(f)$ were deduced as described (Kawai and Brandt

1980). $Y(f)$ was then fitted to Eq. 1 to find the apparent rate constants $2\pi b$ and $2\pi c$. After one or two sets of such analyses, $[MgATP]$ was increased to the next concentration level (0.1, 0.2, 0.5, 1.0, 2.0, 5.0, and 10.0 mM), and sinusoidal analysis was repeated. After challenging with eight different MgATP concentrations, fibers were relaxed in R (Fig. 2B). These experiments were carried out in the presence of the ATP regenerating system, hence contaminating ADP was $< 20 \mu M$ (Kushmerick et al. 1992) and negligible. In the ATP study, $[Pi]$ was kept constant at 8 mM, and pCa was kept in the range of 4.65–4.35 ($[Ca^{2+}] = 22\text{--}45 \mu M$). The experiments for the next preparation were carried out in decreasing order of $[ATP]$, and the results were averaged to minimize the effect of fiber rundown.

Phosphate (Pi) study and analysis of the apparent rate constant $2\pi b$

The Pi study was carried out as in Fig. 2C. To deduce the kinetic constants (r_4 , r_{-4} , K_5) of the elementary steps surrounding force generation (Step 4) and Pi release (Step

Table 1 Solutions used in this report (mM)

Solution name Symbol	Relaxing R	Activating A	Rigor Rig	MgATP study		Pi study	
				0S	10S	0P	30P
K ₂ CaEGTA	–	6	6	6	6	6	6
K ₂ H ₂ EGTA	10	–	–	–	–	–	–
Na ₂ H ₂ ATP	2.4	6.06	–	–	12.1	6.12	6.06
Na ₂ CP	–	15	–	15	15	15	15
MgAc ₂	3.9	6.61	1.55	1.69	11.53	6.68	6.44
KH ₂ PO ₄	4	4	4	4	4	0	15
K ₂ HPO ₄	4	4	4	4	4	0	15
KAc	65	53.5	88.7	74	33.2	72.1	14.5
KCl	12	12	12	12	12	12	12
NaAc	20	12.8	55	25	0.8	12.8	0.9
MOPS	10	10	10	10	10	10	10
CK (unit/ml)	0	80	0	80	80	80	80

CP creatine phosphate, CK creatine kinase. $S = [\text{MgATP}]$, $P = [\text{Pi}]_{\text{total}} = [\text{PO}_4^{1.5-}]$. mS indicates mM concentration (m) of ATP study solutions. Intermediate S solutions are made by an appropriate mixture of 0S and 10S solutions: $nS = [n(10S) + (10-n)(0S)]/10$ by volume. nP indicates the mM concentration (n) of Pi study solutions. Intermediate P solutions are made by an appropriate mixture of 0P and 30P solutions: $nP = [n(30P) + (30-n)(0P)]/30$ by volume. A is the standard activating solution, which is the same as 5S and 8P solutions. In all solutions, pH was adjusted to 7.00 by KOH. $[\text{Mg}^{2+}] = 1$ mM, $[\text{Na}^+]_{\text{total}} = 55$ mM. The ionic strength was adjusted to 200 mM by KAc

5), $[\text{Pi}]$ was changed such as 0, 2, 4, 8, 16, and 30 mM in the experimental saline. Pi was included in the saline as the equimolar mixture of KH₂PO₄ and K₂HPO₄ (Table 1); $P = [\text{Pi}]$ represents the total Pi concentration. The actual Pi concentration was likely to be 0.7–0.8 mM higher than the added concentration because of continuous ATP hydrolysis by the fibers and diffusion of Pi to the surrounding saline (Kawai and Halvorson 1991; Dantzig et al. 1992). The apparent rate constant $2\pi b$ was then studied as a function of $[\text{Pi}]$. $2\pi b$ reflects the force generation and Pi release steps (Kawai and Halvorson 1991; Kawai et al. 1993). Fibers were initially relaxed in R, and then the solution was replaced twice with a solution that did not contain Pi (0 Pi solution). Because R contained 8 mM Pi, the first solution was used to wash out excess Pi. Tension quickly rose to reach a plateau (Fig. 2C), and the fiber length was oscillated for sinusoidal analyses. $[\text{Pi}]$ was then increased to the next concentration level (2, 4, 8, 16, and 30 mM), and sinusoidal analyses were repeated. After sequentially challenging the fibers with six different Pi concentrations, fibers were relaxed in R. In the Pi study, $[\text{MgATP}]$ was kept at 5 mM, and pCa was kept at 4.55 ($[\text{Ca}^{2+}] = 28$ μM). The experiment for the next preparation was carried out in decreasing order of $[\text{Pi}]$, and the results were averaged to minimize rundown artifact.

Ca²⁺ study

This was performed at pCa 7.0, 6.2, 6.0, 5.8, 5.7, 5.6, 5.5, 5.4, 5.2, 4.8, and 4.55 as in Fig. 2D (see also Fig. 1 of Zhang

et al., 2021), where $\text{pCa} = -\log_{10}[\text{Ca}^{2+}]$, and isometric tension was recorded as reported (Lu et al. 2010; Zhang et al. 2021). $[\text{MgATP}]$ was kept at 5 mM and $[\text{Pi}]$ at 8 mM. For each pCa solution, sinusoidal analysis was performed, and the complex modulus was recorded. After the maximum $[\text{Ca}^{2+}]$, the fiber was relaxed with R.

Solutions

Solutions are listed in Table 1, several of which were reported previously (Wang et al. 2013b, 2014). In brief, the relaxing solution (R) contained 10 mM EGTA, 2.4 mM ATP, 4 mM MgAc₂ (Ac = acetate), and 8 mM Pi. Activating solutions contained 6 mM CaEGTA, 0–12 mM ATP, 1.7–12.0 mM MgAc₂, and 0–30 mM Pi. All activating solutions contained the ATP regenerating system: 15 mM Na₂CP (creatine phosphate) and 80 unit/ml CK (creatine kinase). For the pCa study, the ratio $[\text{Na}_2\text{CaEGTA}]:[\text{Na}_2\text{K}_2\text{EGTA}]$ was adjusted to achieve the desired pCa value by keeping the total $[\text{EGTA}]$ constant (6 mM) and by using a program developed in our laboratory, ME.exe (multiple equilibria). This program considers interactions between multiple cations and multiple anions at a specified pH based on the mass action law and published stability constants. The rigor solution contained: 6 mM CaEGTA, 1.55 mM MgAc₂, and 8 mM Pi. In all solutions, $[\text{Mg}^{2+}] = 1$ mM, $[\text{Na}^+]_{\text{total}} = 55$ mM, the ionic strength was adjusted to 200 mM by KAc, and pH was adjusted to 7.00 by KOH. All experiments were carried out at 25 °C.

Statistical analysis

All data are expressed as the mean \pm standard error of the mean (SEM).

Results

Cross-bridge (CB) kinetics during standard activation

This is depicted in Fig. 2A. Fibers were initially soaked in R and then transferred to the standard activating solution (A). Once steady tension developed, the length of the fibers was oscillated with a small amplitude ($0.2\% L_0$). This length change corresponded to ~ 1 nm/CB with 50% series compliance. The concomitant change in tension was recorded every $10 \mu\text{s}$ by a computer with an Advantech PCA-6743F CPU

using our customized interface and analyzed in terms of discrete Fourier transform by using a program developed in our laboratory, Dcoll.exe, and as reported (Kawai and Brandt 1980; Kawai et al. 2021). The complex modulus ($= Y(f)$) was calculated as a function of frequency (f). The results are plotted in Fig. 3. The elastic modulus ($EM = \text{Real } Y(f)$) has a minimum at 17 Hz (Fig. 3A). This frequency is close to the one called “ f_{min} ,” which is defined as the frequency that gives the minimum value on the dynamic modulus $|Y(f)|$ (Shibata et al. 1987). The EM is very large at the high-frequency end (100 Hz) because CBs do not have enough time to adjust to the imposed length change; hence, the EM registers a momentarily frozen structure of the preparation. The EM is small at the low-frequency end (1 Hz) because CBs have adequate time to adjust to the imposed length change. The viscous modulus ($VM = \text{Imag } Y(f)$; Fig. 3B) peaks at 50 Hz, which approximates the characteristic frequency c . Although difficult to see, the VM has a minimum at 5–7 Hz where

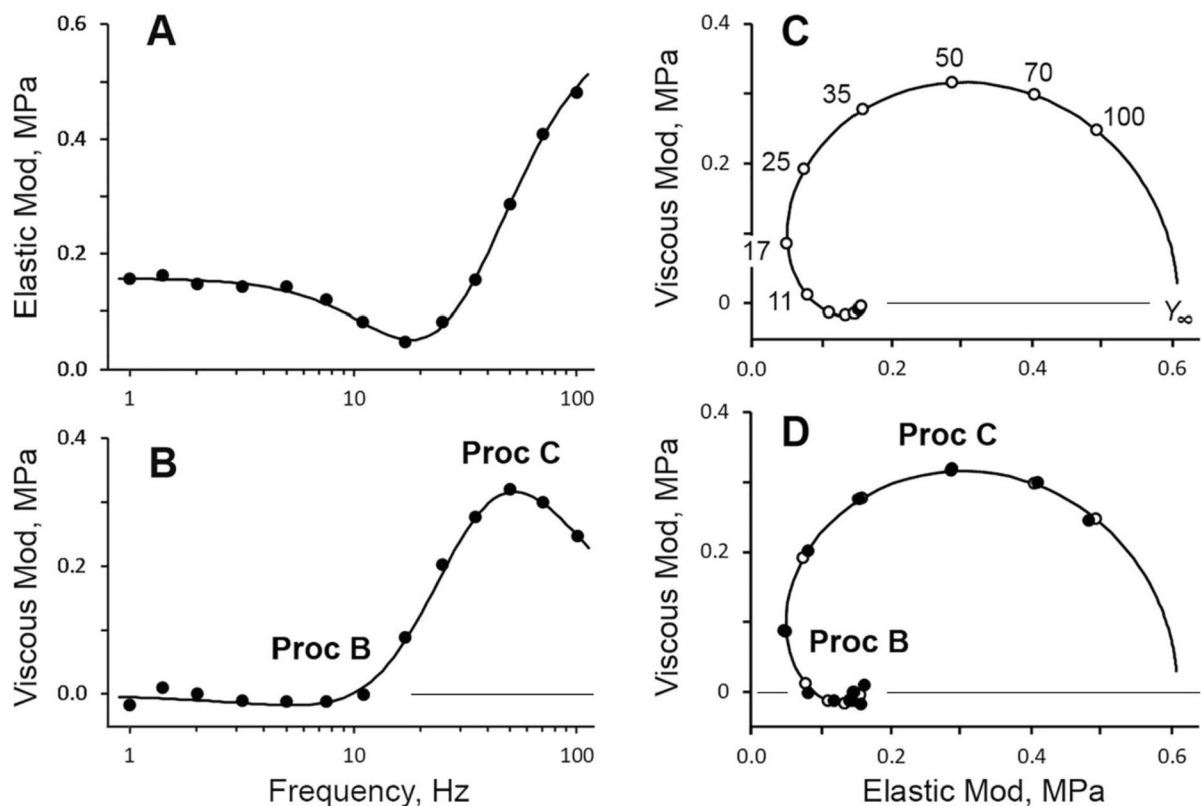


Fig. 3 Plots of complex moduli of standard activation. **A** Elastic modulus vs. frequency. **B** Viscous modulus vs. frequency. **C** and **D** Elastic vs. viscous moduli (Nyquist plot). In **A**, **B** and **D** filled circles represent the experimentally observed data points. Curved lines (and open circles in **C** and **D**) are the theoretical values based on Eq. 1 and best fit parameters. In **C**, theoretical projections based on Eq. 1 (curved line) with frequencies used for measurements (open circles). Frequency points are indicated in Hz in **C**, except for 7.5, 5.0, 3.2, 2.0, 1.4, and 1.0 Hz (counter-clockwise direction), which are not indicated. Y_{∞} is on the point at which the complex modulus extrapo-

lates for $f \rightarrow \infty$. **D** superimposes **C** and the experimentally observed data points shown in **A** and **B**. Many open circles (theory) overlap with solid circles (measurements), hence not all points are visible. The fitting procedure minimized the sum of squares of their distances. Note that the viscous modulus becomes slightly negative for frequencies < 10 Hz (**B**, **C** and **D**). In **B** and **D** approximate locations of Processes B and C are indicated by Proc B and Proc C. The data are based on a single set of measurements and are not averaged. The coefficient of correlation of this fitting was 0.998. The unit of moduli is MPa, and the unit of frequency is Hz

Table 2 CB parameters from standard activation and rigor

Preparations CB parameters	Flash-frozen/cryo-sectioned This report	Ordinary skinned Xi et al. (2022)	Unit
<i>Standard activation</i>			
Tension	16.3 ± 1.1 (42)	26.3 ± 2.1 (66)	kPa
Stiffness	0.53 ± 0.04 (42)	1.16 ± 0.09 (70)	MPa
Tension: Stiffness	3.21 ± 0.14 (42)	2.06 ± 0.11 (66)	%L ₀
Rate Const 2πb	80.3 ± 5.5 (42)	74.1 ± 4.3 (70)	s ⁻¹
Rate Const 2πc	181 ± 9 (42)	154 ± 7 (70)	s ⁻¹
Magnitude H	0.21 ± 0.02 (42)		MPa
Magnitude B	0.487 ± 0.055 (42)		MPa
Magnitude C	0.806 ± 0.067 (42)		MPa
Coefficient of correlation	0.993 ± 0.001 (42)	0.979 ± 0.003 (70)	–
<i>Rigor</i>			
Tension	21.7 ± 1.5 (39)	29.4 ± 2.6 (70)	kPa
EM at 100 Hz	1.01 ± 0.06 (39)	1.86 ± 0.17 (70)	MPa
Tension:EM	2.18 ± 0.10 (39)	1.83 ± 0.10 (70)	%L ₀

The mean, ± SEM, and number of observations are shown in (). The standard activating solution contained 5 mM MgATP and 8 mM Pi, and the ionic strength was 200 mM. pCa 4.55 and pH 7.00

Stiffness = Young's elastic modulus extrapolated to ∞ frequency. The data for ordinary skinned fibers were taken from Xi et al. (2022) after averaging the data for males and females

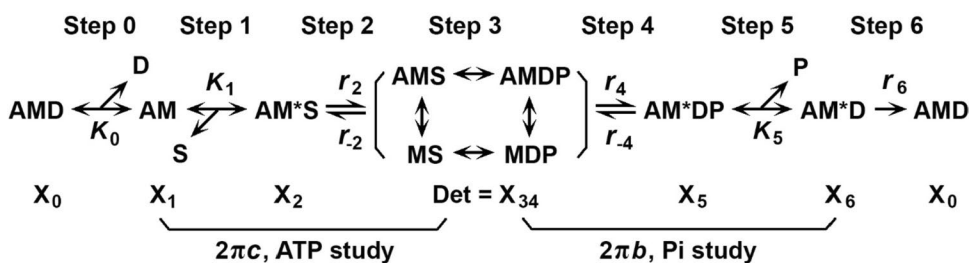


Fig. 4 Cross-bridge (CB) model with six states. The complex modulus data $Y(f)$ were analyzed based on this CB model, where $D = \text{MgADP}$, $S = \text{MgATP}$, $P = \text{Pi} = \text{phosphate}$, $A = \text{actin}$, and $M = \text{myosin}$. Det is an assembly of weakly attached states (AMS and AMDP) and detached states (MS and MDP). X_j ($j=0, 1, 2, 34, 5, 6$)

6) is the probability of CBs in each state. $2\pi c$ represents Steps 0–2, and $2\pi b$ represents Steps 4–5. r 's are the fundamental rate constants, and K 's are the equilibrium constants (including the association constants) of elementary steps

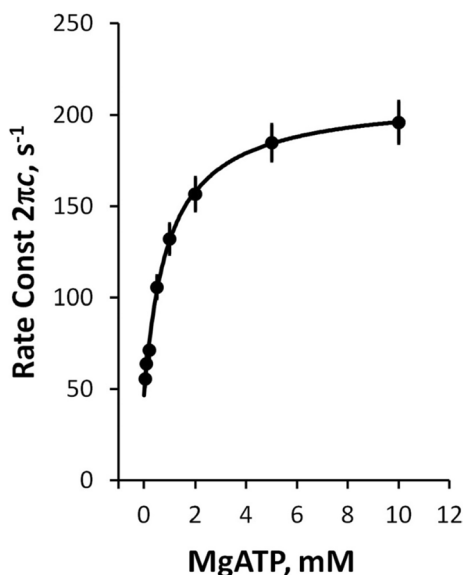


Fig. 5 Effect of MgATP on apparent rate constant $2\pi c$. $[\text{MgATP}] = 0.05, 0.1, 0.2, 0.5, 1, 2, 5, 10$ mM. Experiments were performed at 8 mM Pi and pCa 4.35–4.65. The mean and SEM are shown. $N = 18$. The data were fitted to the three-state model (Eq. 4), that includes Step 1 and Step 2 in Fig. 4

$VM < 0$. This frequency approximates the characteristic frequency b . The muscle preparation produces “oscillatory work” at around this frequency (Pringle 1967; White and Thorson 1972; Kawai et al. 1977; Kawai and Brandt 1980).

Active tension (Table 2) was 16.3 ± 1.1 kPa ($N = 42$), and associated stiffness (Young’s elastic modulus extrapolated to ∞ frequency, Eq. 3) was 529 ± 36 ($N = 42$) in the standard activating solution that contained 8 mM Pi (Table 1). This condition lowers the isometric tension, compared to that at 0 mM Pi (23.8 ± 1.9 kPa, $N = 14$).

The Nyquist plot is a plot of EM in the abscissa vs. VM in the ordinate (Fig. 3C and D). This plot exhibits two semicircles, with the large one opening downward (Process C), and the small one opening upward (Process B). One semicircle

corresponds to one exponential process (compare Eqs. 1 and 2); therefore, these Nyquist plots demonstrate that there are two exponential processes involved in the length-tension response in activated processes cardiac muscles (Kawai et al. 1993; Wannenburg et al. 2000). These are called “exponential” processes, because their time-domain expression consists of exponential functions, as shown in Eq. 2. The quality of the exponential time course is very difficult to judge by its appearance, in particular when there are multiple exponentials; whereas, in Nyquist plots, these are easy to identify and easy to judge the quality of the data because of their circular nature (see Fig. 3C).

To determine the apparent rate constants $2\pi b$ and $2\pi c$, the complex modulus data were fitted to Eq. 1 (Kawai and Brandt 1980; Kawai et al. 1993; Wannenburg et al. 2000). This process is equivalent to fitting the time course data to two exponential functions (Eq. 2) to deduce two apparent rate constants. The sinusoidal analysis method gives a more accurate estimate of the rate constants in a larger frequency (or time) domain. In Fig. 3, the best fit theoretical data (calculated by Eq. 1) are expressed in continuous curves and open circles. Figure 3C is entirely based on Eq. 1, with best fit parameters and frequency points (indicated) used for experiments. Figure 3D superimposes the experimental data points on top of Fig. 3C. The coefficient of correlation of this fitting was 0.998 for a single measurement. This is much better than that determined using data from ordinary single skeletal muscle fibers or cardiac muscle strips (Table 2), because these preparations require the averaging of many $Y(f)$ data for satisfactory results. As demonstrated in Fig. 3D, the data points and theoretical points superimpose extremely well. This can also be seen in Fig. 3A and B (data points are close to the theoretical curves), indicating the high quality of the data and the appropriateness of Eq. 1 to describe the frequency-dependent complex modulus data.

Table 3 Kinetic constants of the elementary steps. The mean, SEM, and number of observations are shown

Preparations	Name	Flash-frozen/cryo-sectioned		Unit
		This report	Xi et al. (2022)	
K_1	ATP association constant	1.03 ± 0.09 (20)	1.12 ± 0.14 (28)	mM^{-1}
r_2	CB detachment RC	163 ± 10 (20)	166 ± 11 (28)	s^{-1}
r_{-2}	Reverse detachment RC	48.3 ± 3.8 (20)	41.2 ± 4.3 (28)	s^{-1}
K_2	CB detachment EC	3.74 ± 0.32 (20)	4.80 ± 0.41 (28)	–
r_4	Force generation RC	64.5 ± 3.7 (14)	49.1 ± 4.2 (19)	s^{-1}
r_{-4}	Reverse force generation RC	87.1 ± 12.9 (14)	77.4 ± 14.1 (19)	s^{-1}
K_4	Force generation EC	0.99 ± 0.16 (14)	1.07 ± 0.21 (19)	–
K_5	Pi association constant	0.200 ± 0.042 (14)	0.172 ± 0.032 (19)	mM^{-1}

RC rate constant, EC equilibrium constant

Rigor study

To determine the significance of stiffness of in-series components, the standard activating solution was washed with the rigor solution (Rig; Fig. 2A), which did not contain ATP, CP or CK (Table 1). Rigor is a condition in which all possible CBs are attached to the thin filament; thus, it is a measure of the stiffness of the overall sarcomere structure. Rigor tension initially increased then gradually decreased (Fig. 2A). The rigor tension reached steady state in a few minutes, and the complex modulus data were collected. Rigor stiffness at $f=100$ Hz was chosen because it varies little with frequency when rigor is developed (Kawai and Brandt 1980). Results are shown in Table 2.

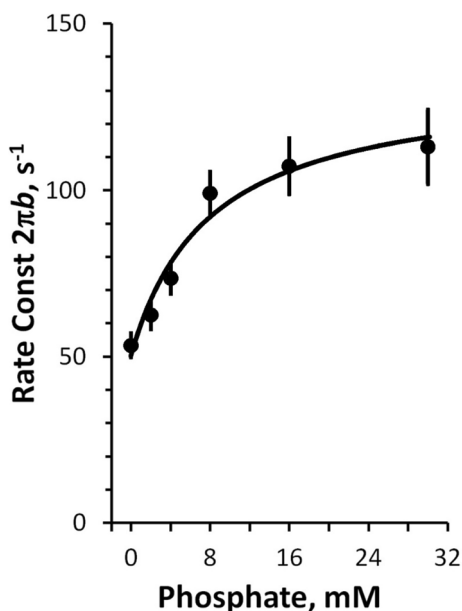


Fig. 6 Phosphate effect on the apparent rate constant $2\pi b$. Experiments were performed at $[\text{MgATP}]=5$ mM and pCa 4.55. The mean and SEM are shown. Average of 18 experiments. The data were fitted to the three-state model (Eq. 5), that includes Steps 4 and 5 in Fig. 4

Elementary steps surrounding ATP binding and CB detachment

The apparent rate constant $2\pi c$ reflects the CB detachment step that rapidly ensues after the ATP binding step (Kawai and Halvorson 1989; Kawai et al. 1993). To characterize these steps, the effect of $[\text{MgATP}]$ on $2\pi c$ was studied in the range of 0.05–10 mM and as shown in Fig. 2B. $2\pi c$ increased as $S = [\text{MgATP}]$ was increased in the sub-mM range and subsequently approached saturation (Fig. 5). These results can be explained by Steps 1 and 2 of the CB model shown in Fig. 4. Equation 4 relates $2\pi c$ to the MgATP concentration ($S = [\text{MgATP}]$) and to the kinetic constants (K_1, r_2, r_{-2}) of the elementary steps (Kawai and Halvorson 1989).

$$2\pi c = \frac{K_1 S}{1 + K_1 S} r_2 + r_{-2} \quad (4)$$

The data points are fitted to Eq. 4 by a program developed in our laboratory, F_Sr6, which minimizes the sum of squares by using a one-dimensional search for K_1 . r_2 and r_{-2} are linear to $2\pi c$, hence ordinary linear fitting was used. From this fitting three kinetic constants (K_1, r_2 , and r_{-2}) of the elementary steps are deduced. K_1 is the MgATP association constant (Step 1), r_2 is the rate constant of the CB detachment Step 2, and r_{-2} is the rate constant of its reversal (see Fig. 4). The data (discrete points) fit well to Eq. 4 as shown in the smooth curve of Fig. 5, demonstrating the high reliability of the CB model. Here it is important to emphasize that we have derived only three parameters (K_1, r_2 , and r_{-2}) from the ATP experiment (Fig. 5), and we interpret them in terms of elementary Steps 1 and 2 of Fig. 4, which is the minimal CB model. Therefore, this is the simplest interpretation of the data. The isometric tension gradually decreased (Fig. 2B) as $[\text{MgATP}]$ was increased, and as reported previously (Kawai and

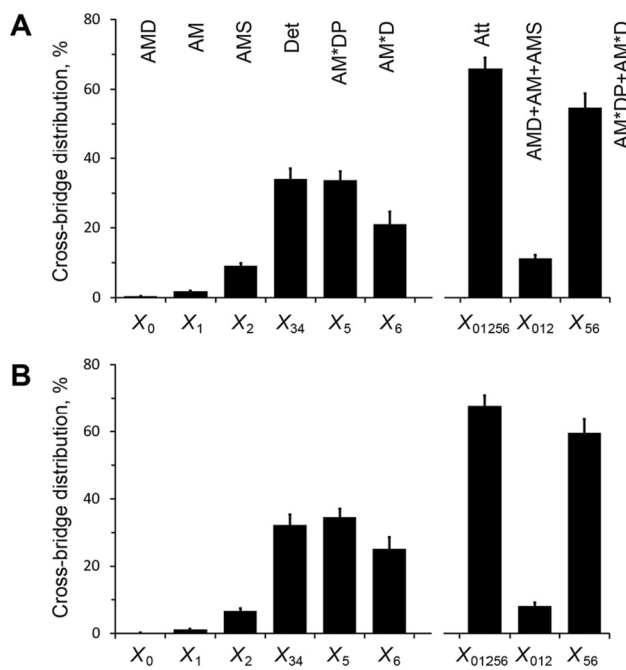


Fig. 7 Cross-bridge distribution. **A** Flash-frozen and cryo-sectioned preparation. **B** Ordinary preparation. CB states on top follow the abbreviations used in Fig. 4. CB distribution was calculated from equilibrium and association constants in Table 3 at $S=5$ mM, $P=8$ mM, and $D=[\text{MgADP}]=0.02$ mM, based on Eqs. 8–14 of Zhao & Kawai (1996). Errors were propagated from SEM listed in Table 3. $\text{Att}=\text{AMD}+\text{AM}+\text{AMS}+\text{AM*DP}+\text{AM*D}=\text{X}_0+\text{X}_1+\text{X}_2+\text{X}_5+\text{X}_6=\text{X}_{01256}$. These are force generating, strongly attached states. X_{34} is an assembly of detached and weakly attached states without force, and $\text{X}_{01256}+\text{X}_{34}=1$. To calculate X_0 , $K_0 \approx 10K_1$ and $[\text{MgADP}] \approx 0.02$ mM were assumed. $\text{X}_0 \approx 0.36 \pm 0.03\%$ for **A** and $0.27 \pm 0.03\%$ for **B**. $\text{X}_{012}=\text{X}_0+\text{X}_1+\text{X}_2$; $\text{X}_{56}=\text{X}_5+\text{X}_6$

Halvorson 1989; Wang et al. 2014). The results of the ATP study are summarized in Table 3.

Elementary steps surrounding force generation and phosphate (Pi) release

The apparent rate constant $2\pi b$ reflects the force generation and the Pi release steps (Kawai and Halvorson 1991; Kawai et al. 1993). To characterize these steps, $P=[\text{Pi}]_{\text{total}}$ was changed in the range of 0–30 mM, and $2\pi b$ was recorded. The results are plotted in Fig. 6 (discrete points) as a function of P . $2\pi b$ increased at a low concentration of Pi and approached saturation at a high concentration range. Such a result can be explained by force-generations Step 4 and Pi-release Step 5 of the CB model depicted in Fig. 4. The effect of Pi on $2\pi b$ is fitted to Eq. 5 by a program developed in our laboratory, F_PR6C, which minimizes the sum of squares by using a one-dimensional search for K_5 , r_4 and r_{-4} are linear to $2\pi b$, hence ordinary linear fitting was used. This

equation is based on Steps 4 and 5 of Fig. 4, and relates the Pi concentration (P) and the kinetic constants (r_4 , r_{-4} , K_5) of elementary Steps 4 and 5 to the apparent rate constant $2\pi b$ (Kawai and Halvorson 1991; Kawai et al. 1993):

$$2\pi b = \sigma r_4 + \frac{K_5 P}{1 + K_5 P} r_{-4} \quad (5)$$

where

$$\sigma \equiv \frac{K_2 K_1 S}{1 + (1 + K_2) K_1 S} \quad (6)$$

σ accounts for the rapid equilibria (Steps 1–3, Fig. 4) that exist to the left of Step 4. K_1 and K_2 were obtained from the ATP study, and $S=5$ mM (condition of the Pi study) was used to calculate σ from Eq. 6. The data fit well to Eq. 5, as shown in the continuous curve in Fig. 6, demonstrating the high reliability of the CB model in Fig. 4. Once again it is important to emphasize that we have deduced only three parameters (r_4 , r_{-4} , and K_5) from the Pi study, showing Pi dependence of $2\pi b$ (Fig. 6); hence, Fig. 4 with Steps 4 and 5 is the minimal CB model to account for the data. The isometric tension gradually decreased as $[\text{Pi}]$ was increased (Fig. 2C), and as reported earlier (Hibberd et al. 1985; Kawai and Halvorson 1991; Kawai et al. 1993; Tesi et al. 2000; Wang et al. 2014). The results of the Pi study are summarized in Table 3.

Distribution of CBs among six states

It is important to know how CBs are distributed among the six states shown in Fig. 4, and how they change depending on $S=[\text{MgATP}]$ and $P=[\text{Pi}]$. The CB distribution was calculated based on equilibrium constants that include the association constants obtained (K_1 , K_2 , K_4 and K_5 in Table 3) at the standard activating condition ($S=5$ mM, $P=8$ mM and $D=0.02$ mM) using Eqs. 8–14 published in (Zhao and Kawai 1996) based on the CB model in Fig. 4 and plotted in Fig. 7A. Because we have not performed the ADP study from which K_0 (MgADP association constant) is determined, $K_0 \approx 10K_1$ was assumed for the ratio of K_0/K_1 resulted in a range between 6–14 in cardiac preparations (Lu et al. 2003, 2005; Wang et al. 2013a; Bai et al. 2014), indicating that ADP binds about 10 times more strongly than ATP to the nucleotide binding site of myosin in cardiac muscle fibers. $D=[\text{MgADP}]$ in the presence of CP/CK is ≤ 0.02 mM (Kushmerick et al. 1992), but we used $D=0.02$ mM to indicate the upper limit of the associated state ($\text{X}_0=(\text{AMD})$). However, the exact values for K_0 and D do not matter much, because $\text{X}_0=K_0 \text{DX}_1$, which is a small value compared to X_1 , which itself is small ($<2\%$, Fig. 7A). Errors were propagated based on SEM for each kinetic constant. This plot

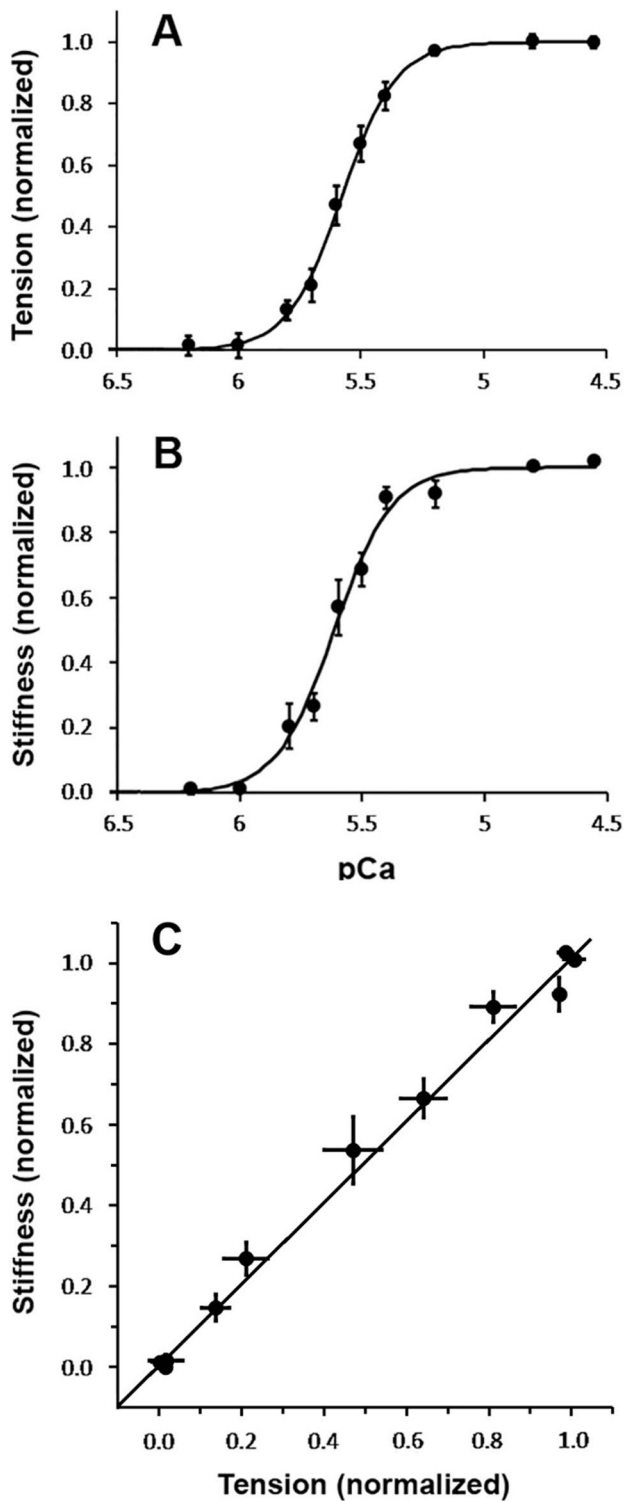


Fig. 8 Effect of pCa, where $pCa = -\log_{10}[Ca^{2+}]$. **A** on Tension, and **B** on Stiffness (Y_{∞}). Each pCa-tension (or stiffness) curve was fitted to Eq. 7 (Eq. 8), followed by subtracting T_{LC} (Y_{LC}) and dividing the result by T_{act} (Y_{act}). The data were then averaged for 13 experiments and plotted with SEM. **C** Tension vs. Stiffness plot of the same data. The straight line is drawn to show the equality, and it is not the regression line. Some SEM error bars are smaller than the symbol size and cannot be seen

Table 4 Results of the pCa study at 5 mM MgATP, 8 mM Pi, and 200 mM IS

Preparations	Flash-frozen/cryo-sectioned	Ordinary skinned
Parameters	This report	Xi et al. (2022)
<i>Based on Tension</i>		
pCa ₅₀ , Ca ²⁺ sensitivity	5.576 ± 0.031 (13)	5.602 ± 0.025 (24)
n _H , cooperativity	4.6 ± 0.4 (13)	4.0 ± 0.4 (24)
T _{act} , maximum tension	14.5 ± 2.3 kPa (13)	
cc, coefficient of correlation	0.984 ± 0.006 (13)	
<i>Based on stiffness</i>		
pCa _{50Y} , Ca ²⁺ sensitivity	5.584 ± 0.027 (13)	
n _{HY} , cooperativity	4.9 ± 0.5 (13)	
Y _{act} , maximum stiffness	0.48 ± 0.06 MPa (13)	
cc, coefficient of correlation	0.991 ± 0.003 (13)	

The mean, SEM, and the number of observations are shown

The data were fitted to Eq. 7 (Tension) or Eq. 8 (Stiffness) by using a program developed in our laboratory, F_pCaTS.exe for both tension and stiffness. There was no significant difference in pCa₅₀ or n_H values regardless whether the tension or the stiffness data were used. Total number of data points: 100 each of tension and stiffness

demonstrates that most of the CBs are distributed among the detached states (Det, X₃₄: 34%), and in the strongly attached states before (AM*ADP.Pi, X₅: 34%) and after (AM*ADP, X₆: 21%) the Pi release Step 5 (total is X₅₆: 55%). The distribution of CB states in AM.ADP, AM, and AM.ATP (total is X₀₁₂: 11%) is small. These are the states that exist after work performance. The force generating or force bearing (strongly attached) states (X_{att}) are the summation of X₀₁₂ and X₅₆.

Comparison to ordinarily skinned cardiac fiber preparations

To compare the current results with ordinary preparations, the data published in (Xi et al. 2022) are most suitable, because experiments were performed by the same person (JX) with the same experimental apparatus and under the same experimental conditions on C57BL/6 mouse cardiac preparations. These data are listed in Table 2 and 3 after averaging the results for females and males. The results show that rigor and active stiffness (elastic modulus) in frozen preparations were each reduced to about 1/2. The stiffness decreased more than tension, resulting in an increase in the tension:stiffness ratio (Table 2). Changes in the apparent rate constants ($2\pi b$ and $2\pi c$) are almost negligible (Table 2). Changes in the kinetic constants of the elementary steps are almost none (Table 3). The CB distribution was calculated similar to Fig. 7A, and plotted in Fig. 7B. This plot demonstrates that the CB distribution is identical between frozen and ordinary preparations.

pCa-tension study and Ca^{2+} sensitivity

This was carried out as described in the Methods section and as depicted in Fig. 2D. The results are plotted as discrete points in Fig. 8A. There was no noticeable active tension at pCa 8.0–6.5, and the muscle was relaxed. Tension increased in a sigmoidal manner as $[\text{Ca}^{2+}]$ was increased (pCa: 6.0–5.5), and it reached saturation by pCa 5.30–4.55. The pCa-tension curve was fitted to the Hill equation (Eq. 7) (Hill 1910) using a program developed in our laboratory, F_pCaTSc.exe, which minimizes the sum of squares by performing a two-dimensional search for Ca_{50} and n_H . T_{LC} and T_{act} are linear to *Tension*, hence ordinary linear fitting was used.

$$Tension = T_{LC} + \frac{T_{act}}{1 + \left(\frac{\text{Ca}_{50}}{[\text{Ca}^{2+}]}\right)^{n_H}} \quad (7)$$

where T_{LC} = low $[\text{Ca}^{2+}]$ tension during relaxation for pCa 8.0–6.5 measured on the chart paper, T_{act} = the amount of

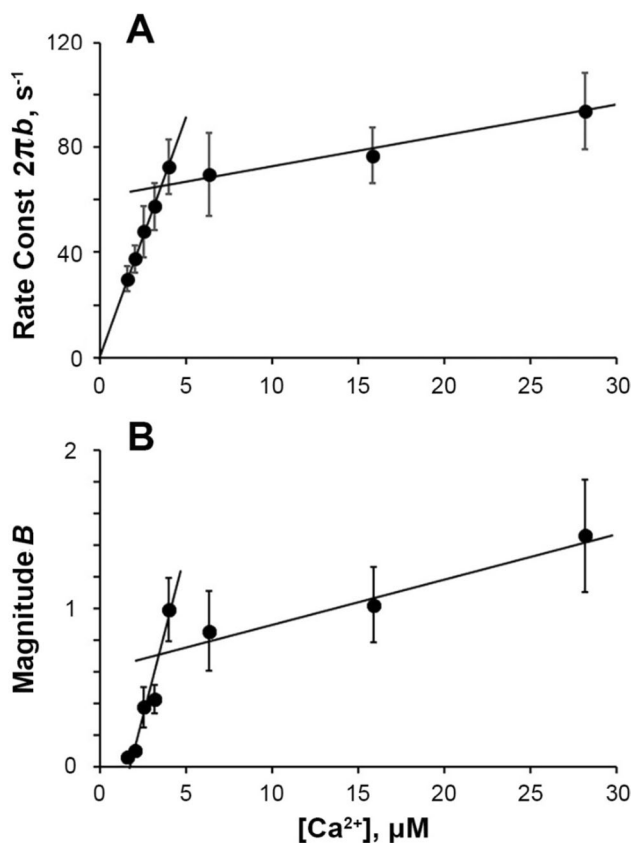


Fig. 9 Effect of $[\text{Ca}^{2+}]$ (linear scale) on exponential Process B. **A** on the apparent rate constant $2\pi b$, and **B** on the magnitude B. Before averaging, B was normalized (divided) by Y_{act} of the standard activation. The average of 12 measurements with SEM are shown. Lines are drawn by eye to show the trend of the data

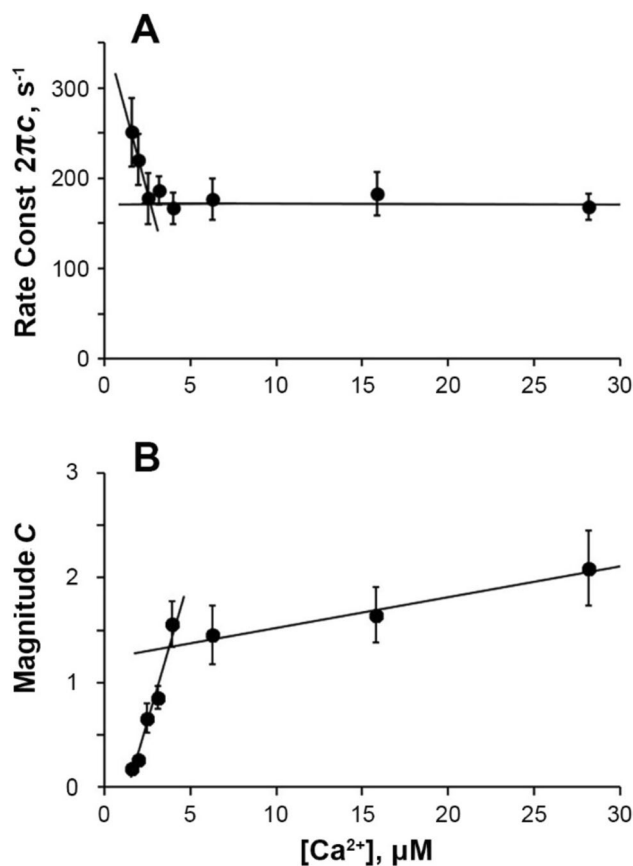


Fig. 10 Effect of $[\text{Ca}^{2+}]$ on exponential process C. **A** on $2\pi c$, and **B** on magnitude C. The data were similarly treated as in Fig. 9. The unit of C is Y_{act} . Lines are drawn by eye to show the trend of the data

tension activated by Ca^{2+} , $\text{Ca}_{50} = [\text{Ca}^{2+}]$ at 50% T_{act} , and n_H = cooperativity (Hill coefficient). Ca_{50} is the apparent Ca^{2+} dissociation constant, and $\text{pCa}_{50} = -\log_{10}\text{Ca}_{50}$ is called “Ca sensitivity.” Each pCa-tension curve was first fitted to Eq. 7 to determine T_{LC} , T_{act} , Ca_{50} , and n_H for each experiment. This procedure was followed by subtracting T_{LC} from tension data, and then dividing the result by T_{act} for normalization. The normalized data were then averaged for multiple pCa-tension measurements and plotted in Fig. 8A with SEM. The averaged fitted parameters are listed in Table 4. Ca^{2+} sensitivity (pCa_{50}) was found to be 5.576 ± 0.031 ($N = 13$), with cooperativity (n_H) of 4.6 ± 0.4 , and active tension (T_{act}) of 14.5 ± 2.3 kPa. The averaged coefficient of correlation was 0.984 ± 0.006 . The curved line is the theoretical curve based on Eq. 7 with best fit parameters. As seen in Fig. 8A, Eq. 7 explains the pCa-tension data well. The results are compared to those obtained from ordinary skinned fiber preparations (Table 4). This comparison demonstrates that Ca^{2+} sensitivity and cooperativity are respectively not any different between frozen and ordinary skinned preparations.

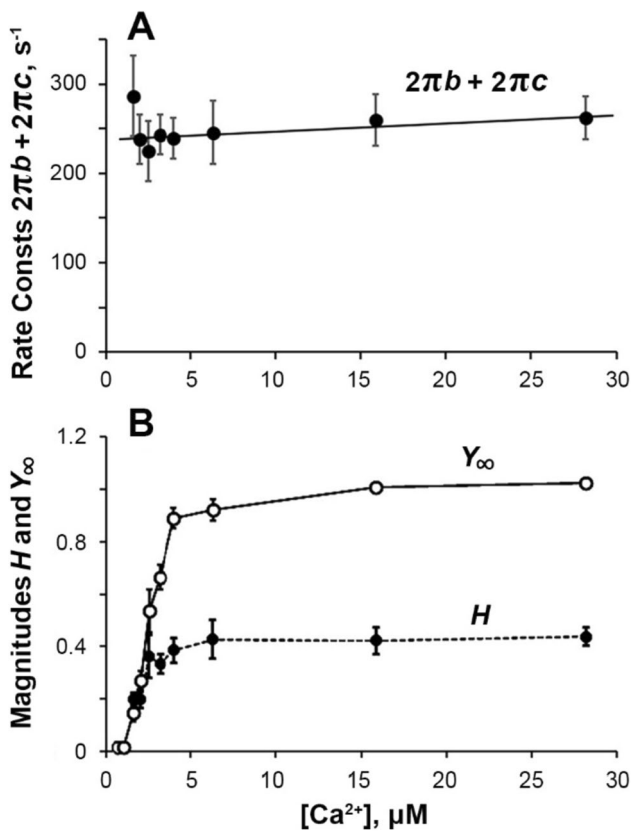


Fig. 11 Effect of Ca^{2+} on exponential processes. **A** on the sum $2\pi b + 2\pi c$. Line is drawn by eye to show the trend of the data. **B** Effect of Ca^{2+} on H and Y_{∞} with the unit Y_{act} . Lines are drawn to connect data points. Y_{∞} is the same data as those plotted in Fig. 8B in log (pCa) scale

pCa-stiffness results

The pCa-tension data were sometimes scattered, which was mostly caused by the shape of the meniscus of the pin that connects muscle fibers to the tension transducer; we measure small force $\sim 1 \mu N$ (about 0.1 mg-wt force). With our method, each pCa solution is kept in a different muscle chamber, hence the preparation and the pins have to cross the meniscus each time the solution is changed; a small variation in the shape of the meniscus interferes with the force measurement. In contrast, stiffness (Y_{∞}) is less sensitive to surface tension and often yields better results. For this reason, the pCa-stiffness data were processed similarly to the tension data. An equation similar to Eq. 7 was used to fit the stiffness data to find Y_{LC} , Y_{act} , Ca_{50Y} , and n_{HY} using a program developed in our laboratory, F_pCaTSc.exe (described above):

$$Stiffness = Y_{LC} + \frac{Y_{act}}{1 + \left(\frac{Ca_{50Y}}{[Ca^{2+}]}\right)^{n_{HY}}} \quad (8)$$

This fitting yielded $pCa_{50Y} = 5.584 \pm 0.027$, $n_{HY} = 4.9 \pm 0.5$, $Y_{act} = 0.48 \pm 0.06$ MPa, and coefficient of correlation $= 0.991 \pm 0.003$ ($N = 13$) (Table 4). Consequently, the fitting was slightly better with stiffness than with tension. Statistically, pCa_{50Y} and n_{HY} values are not significantly different from the respective values of pCa_{50} and n_H obtained from the tension data. Figure 8B shows the averaged result from the stiffness data and the theoretical curve based on Eq. 8. From these results it can be inferred that Eq. 8 fits the stiffness data well, indicating the appropriateness of Eq. 8 for describing pCa-stiffness data. Figure 8C shows Tension vs. Stiffness plot of the same data, demonstrating that these are approximately proportionately related under the experimental conditions we used. These results justify the use of the pCa-stiffness data to evaluate Ca^{2+} sensitivity and cooperativity. In this report, magnitude parameters (H , B , C , Y_{∞}) are normalized (divided) by the Y_{act} of the standard activation, where Y_{act} is experimentally nearest Y_{∞} at pCa 4.55, 5 mM MgATP, and 8 mM Pi, and is defined by Eq. 8. Consequently, the unit of magnitude parameters is Y_{∞} .

CB kinetics as the function of $[Ca^{2+}]$

We carried out sinusoidal analysis during the pCa study, and the kinetic parameters are summarized in Figs. 9–11. The apparent rate constant $2\pi b$ is plotted in Fig. 9A, and $2\pi c$ is plotted in Fig. 10A using the linear $[Ca^{2+}]$ scale in μM . The straight lines were entered by eye to show the trend of the data. The data in Fig. 9A did not fit to a typical hyperbolic saturation equation because of the sharp inflection point in the data at $\sim 5 \mu M$ $[Ca^{2+}]$. This inflection divides the data into two sections: 5 points for $[Ca^{2+}] < 5 \mu M$ (rising phase), and 3 points for $[Ca^{2+}] > 5 \mu M$ (saturation phase: three points are not significantly different). The rising phase of $2\pi b$ appears to extrapolate to the origin (Fig. 9A). A similar trend is seen with magnitude parameter B (Fig. 9B), but the line of the rising phase does not go through the origin. In principle, B should have a positive (or 0) intercept as $[Ca^{2+}] \rightarrow 0$ (see below); hence, the plot must be curved near the origin. All the magnitude parameters (H , B , C , Y_{∞}) are divided, or “normalized,” by the Y_{act} (defined by Eq. 8) of full activation at pCa 4.55, 5 mM MgATP, and 8 mM Pi.

As $[Ca^{2+}]$ was increased, the apparent rate constant $2\pi c$ (Fig. 10A) decreased at $[Ca^{2+}] < 5 \mu M$, and was saturated at $[Ca^{2+}] > 5 \mu M$. At the same time, magnitude C (Fig. 10B) increased steeply at $[Ca^{2+}] < 5 \mu M$ and approached saturation at $[Ca^{2+}] > 5 \mu M$; this latter effect was similar to that of magnitude B in Fig. 9B. The sharp increase in $2\pi b$ and the decrease in $2\pi c$ appear to be a mirror image, so their sum $2\pi b + 2\pi c$ was calculated and plotted in Fig. 11A. This plot shows that the sum is almost constant, except for the lowest

[Ca²⁺] point at 1.58 μ M. Figure 11B plots magnitude H and Y_{∞} . Both plots show the normal saturation curves, except at a very low [Ca²⁺]. In principle, these magnitude parameters (H , B , C , Y_{∞}) should have a zero (0) intercept as [Ca²⁺] \rightarrow 0 (no activation), similar to the pCa-tension plot (Fig. 8A); thus, the plots must be curved for [Ca²⁺] between 0 and 1.58 μ M.

Discussion

Advantages of flash-frozen and cryo-sectioned preparation for biomechanical studies

We have used flash-frozen and cryo-sectioned cardiac muscle preparations to examine its usefulness in biomechanical study. We examined the functional integrity of the preparations by studying force transients in response to sinusoidal length changes and by following concomitant elastic and viscous responses in a force–time course at varying frequencies. We have shown microscopic images of such preparations to demonstrate structural integrity (Fig. 1). We used 70- μ m-thick and 50–100- μ m-wide preparations to study cross-bridge (CB) kinetics; we activated the preparations by saturating Ca²⁺ and varying concentrations of ATP and phosphate (Pi). Our results demonstrate excellent CB kinetics with reduced noise and well-defined exponentials, which are better than results collected from ordinary skinned fibers. There are two advantages of using this preparation. First, samples prepared using this technique are easier to handle than single myofibrils. Second, the prepared muscle strips are uniform in both cross-sectional area and perfusion effect, which allows for accurate and reproducible biomechanical measurements, in contrast to ordinarily skinned preparations. This feature is especially valuable for kinetic studies of a cardiac muscle preparation. This preparation was introduced recently by Feng and Jin (2020). It promises to offer the features of muscle prepared using uniform cross-sectional areas, and the prepared muscle samples are easy to transport and exchange among collaborating laboratories around the world.

Comparison to ordinary skinned fibers

Our results are compared to those of ordinary skinned fiber preparations from mouse papillary fibers recently published by (Xi et al. 2022). The most notable effect with flash-frozen and cryo-sectioned preparation is that, during rigor and during activation, stiffness (Young's elastic modulus) decreased to about 1/2 that of ordinary skinned preparation (Table 2), doubling series compliance. In comparison, the effect on active tension was less, and it decreased to 62%

(= 16.3/26.3), resulting in an increase in the tension:stiffness ratio (Table 2). The primary reason for the reduced active tension must be related to the decrease in series stiffness, because the elementary force generated in Step 4 and series stiffness are proportionately related (Zhang et al. 2021). In spite of these changes, CB kinetics are not very much affected by freezing (Table 2 and 3), which results in little difference in CB distribution (compare Fig. 7A vs. B). Ca²⁺ sensitivity or cooperativity is not affected at all (Table 4). Our results demonstrate that the basic contractile function is not altered by flash-frozen and cryo-sectioned preparations, suggesting that the CB's converter domain is little affected by freezing.

Change in series compliance.

The series compliance includes CBs, thick and thin filaments, and Z-line, and it may have a contribution from titin (connectin), but it is not immediately apparent which one of these is responsible for the change. It is likely that the major effect is on CB compliance (such as lever arm). If the effect is outside of CBs (such as the thin filament), then CB cycles many times to stretch series compliance to the point of high force. Because series compliance is generally nonlinear, and stiffness increases at larger stretch, force may not diminish as observed.

Piroddi et al. (2007) studied fresh and frozen myofibrils from human hearts (both atria and ventricles) during Ca²⁺ activation, and did not find any changes in kinetic parameters k_{act} , k_{TR} , or slow and fast k_{REL} . Their results are consistent with ours in that the kinetic constants are not affected by freezing (Table 2 and 3). Jalal and Zidi (2018) studied a large block (12 \times 3.5 \times 6 mm, or 10 mm cube) of porcine bicep femoris muscles and compared fresh vs. cryopreserved (frozen) preparations. They found that longitudinal Young's elastic modulus was smaller (about 1/2) in frozen preparations compared to that of fresh preparations upon stretching. This result is consistent with our results that the stiffness is about 1/2 of ordinarily skinned preparations. But the condition of their preparation, in particular, the degree of rigor development (or activation) was not assessed, which would make a large difference in results.

There may be yet another possibility that some muscle fibers were cut obliquely (or completely) during the cryo-sectioning process, consequently, the number of active fibers may be reduced resulting in a decreased tension and stiffness. We have minimized this possibility by (1) aligning the cryo-sections along the fiber direction and eliminating sections with cut fibers, and (2) by objectively selecting fibers with tension reproducibility of $\geq 90\%$ (cut fiber preparation would have deteriorated quickly with a few activations).

CB kinetics of cryo-sectioned preparations

In contrast to ordinary skinned fibers, we were able to obtain high-quality data that fit well to a simple two-exponential process model (Eq. 1 and Fig. 3), in particular, at a high frequency range, where Process C is resident. Consequently, Process C is better defined in the flash-frozen and cryo-sectioned preparations than in ordinary skinned preparations. Similar improvement in the quality of Process C was observed with single myofibril experiments (Kawai et al. 2021). Evidently, the order of the simplification of preparations is: whole muscle > muscle strips > muscle fibers > cryo-sectioned preparations > myofibrils. Thus, gradual improvement of Process C must be related to the simplification of the preparation—which suggests to us that the extracellular matrix (ECM) is a major cause of the distortion of Process C. The ECM includes sarcolemma and associated collagen fibers, as well as blood vessels and other ECM molecules and structures. It is easy to imagine that these structures interfere with the fast Process C, making it appear as a distributed rate constant, because water molecules have to move in and out of ECM elements as the fiber length is oscillated, thus serving as an extra damping element.

Process C corresponds to Phase 2 of step analysis, and these two methods observe the same molecular events, or elementary steps, in the CB cycle. In fact a possibility of existence of multiple exponential processes was suggested by several investigating groups. Abbott and Steiger (1977) and Kawai et al. (1993) fitted this phase to two exponentials, while Ford et al. (1977) fitted this phase to four exponentials, all in fast twitch fibers. The observation of the multiple exponentials is universal whether based on step analysis (Abbott and Steiger 1977; Ford et al. 1977) or on sinusoidal analysis (Kawai et al. 1993), and not because of nonlinearity involvement of force response at large step amplitudes. The results from these preparations were likely mixed with the effects from passive components such as ECM, as discussed above and as proposed by Abbott and Steiger (1977).

Elementary steps of the CB cycle

One positive aspect is that we were able to deduce the same CB model (Fig. 4) regardless whether cryo-sectioned cardiac strips or ordinary skinned fibers were used (Table 2 and 3, Fig. 7). This fact confirms the universality of the proposed CB model shown in Fig. 4 and experimentally measured rate constants of elementary steps. By comparing stiffness data during standard activation (0.53 ± 0.04 MPa, Table 2) and in rigor (1.01 ± 0.06 MPa), it can be concluded that about $52 \pm 9\%$ ($=0.53/1.01$ with error propagation) of CBs are made during standard activation. This number compares well to the distribution of CBs at X_{56} ($54 \pm 6\%$, Fig. 7A), which includes the AM*ADP.Pi (AM*DP) and AM*ADP

(AM*D) states and is calculated based on the kinetic constants measured in this report (Table 3). The attached CBs may include other strongly attached states (AM.ADP, AM, and AM.ATP), but their sum (X_{012}) is $11 \pm 1\%$ (Fig. 7), and they do not significantly change the results.

Because of the presence of series stiffness, the estimate of CB numbers based on stiffness becomes less sensitive when a larger number of CBs are formed, such as in the rigor condition. In other words, the CB number at rigor state based on stiffness may be an underestimate. Consequently, our estimate of attached CBs during standard activation ($52 \pm 9\%$) is an upper limit, and the actual number may be less. The effect of series stiffness was analyzed by (Wang and Kawai 1997; Pinzauti et al. 2018).

What is important here is that the number of attached CBs is not as small as the 5%–10% that was estimated from the duty ratio using in vitro motility assay experiments (Harris and Warshaw 1993; Webb et al. 2013). The *in-vitro* experiments were performed when the contractile proteins were not tightly packed as in the structured muscle fiber system, hence they may lack allosteric interactions between macromolecules. It is possible that the presence of tight molecular coupling in a fiber system makes a difference from that in an in vitro system. The ionic strength of the activating solution is much less in in vitro assays (≤ 50 mM) compared to fiber studies (~ 200 mM), which may also make a difference.

Partial Ca^{2+} activation and its effect on Process B

Our results demonstrate that regardless whether active tension or stiffness is used, we arrive at the same Ca^{2+} sensitivity and cooperativity results (Fig. 8A and B, Table 4). This fact is convenient when the tension data are not as reliable as the stiffness data at a small force level $1 \mu\text{N}$ (about 0.1 mg-wt force), where the shape of the meniscus interferes with force measurements. This fact implies that tension and stiffness are proportionally related approximately, as shown in Fig. 8C. However, the proportionality of these parameters depends on the experimental conditions, and tension and stiffness are not necessarily proportionally related in all conditions: Tension:Stiffness ratio is $3.21 \pm 0.14\%L_0$ during standard activation (pCa 4.55), but it is $2.18 \pm 0.10\%L_0$ during rigor (Table 2). The ratio is the reciprocal of the slope of Fig. 8C before normalization.

In partial Ca^{2+} activation, it is interesting to note that, as $[\text{Ca}^{2+}]$ is decreased below $5 \mu\text{M}$, the rate constant of Process B ($2\pi b$) decreases (Fig. 9A), whereas that of Process C ($2\pi c$) increases (Fig. 10A), therefore, the two exponential Processes B and C become further apart and more dissociated. This fact implies that Processes B and C represent two different molecular steps, as has been hypothesized (Kawai and Halvorson 1991). The correlation between Process C and the detachment

step is demonstrated by the ATP study on $2\pi c$ (such as in Fig. 5). The correlation between Process B and the force generation step is demonstrated by the Pi study on $2\pi b$ (such as in Fig. 6). Our earlier assumption that Process B represents the force generation step (Kawai and Halvorson 1991) is consistent with the result of the pressure-release experiment (Fortune et al. 1991), caged Pi experiment (Dantzig et al. 1992; Walker et al. 1992), and single molecule experiment (Woody et al. 2019).

What is interesting is that, at a low Ca^{2+} activation (at the rising phase of the pCa-tension curve), a plot of $[\text{Ca}^{2+}]$ vs. $2\pi b$ is linear, and it goes through the origin: $2\pi b$ is proportionate to $[\text{Ca}^{2+}]$ (Fig. 9A). As discussed above, $2\pi b$ represents the force generation Step 4 (Eq. 5, Fig. 4). Its proportionate relationship with $[\text{Ca}^{2+}]$ at $< 5 \mu\text{M}$ (Fig. 9A) indicates that the Ca^{2+} activation mechanism can be approximated by a second order reaction:

$$r_4 = r_{40}[\text{Ca}^{2+}] \quad (9)$$

This would be an empirical equation to relate the Ca^{2+} activation mechanism to the force generation step; a similar mechanism was proposed by Julian (1969) and r_{40} was called as the “activation factor”. For $[\text{Ca}^{2+}] > 5 \mu\text{M}$, this activation mechanism approaches saturation (Fig. 9A). Actual activation starts from Ca^{2+} binding to TnC, and continues with subsequent intermolecular interactions with TnI, TnT, Tpm, actin, and myosin, which are tightly coupled and strongly allosteric. These in turn result in a steep pCa-tension (or pCa-stiffness) relationship (Fig. 8), with the Hill coefficient (n_H) amounting to 4–5 (Table 4). Compared to this high order coupling, the mechanism expressed in Eq. 9 is a very simple relationship between $[\text{Ca}^{2+}]$ and the rate constant of force generation step (r_4), and may be useful for modeling the Ca^{2+} activation mechanisms.

Effect of Ca^{2+} on Process C

The apparent rate constant $2\pi c$ represents the CB detachment Step 2 (Eq. 4, Figs. 4 and 5) (Kawai and Halvorson 1989). Because the effect of $[\text{Ca}^{2+}]$ on $2\pi c$ is relatively small (Fig. 10A) compared to that on $2\pi b$ (Fig. 9A), we conclude that the major effect of Ca^{2+} is on Process B, and its effect on Process C may be secondary and can be caused by the interaction with its effect on Process B. Consequently, we do not state that $[\text{Ca}^{2+}]$ affects CB detachment Step 2, nor that detachment is lessened as $[\text{Ca}^{2+}]$ is increased up to $5 \mu\text{M}$. The fact, that their sum ($2\pi b + 2\pi c$) does not vary much for most of the $[\text{Ca}^{2+}]$ studied (Fig. 11A), suggests that the effect of Ca^{2+} on Process C may be indeed secondary. The fact that $2\pi c$ decreases when $[\text{Ca}^{2+}]$ is increased does not support the model proposed by (Huxley and Simmons 1971;

Huxley 1974) that Phase 2 of the tension transient in step analysis (Process C in sinusoidal analysis) represents the force generation step.

Effect of Ca^{2+} on magnitude H and the low-frequency component

The magnitude parameter H is a constant in Eq. 1, which is the elastic modulus extrapolated to the zero frequency ($f \rightarrow 0$). In cardiac preparations, such as that used in this report, H has a substantial value (Fig. 11B) amounting to 40% of Y_{act} (Table 2). Furthermore, we found that H is $[\text{Ca}^{2+}]$ sensitive (Fig. 11B) and becomes activated, similar to tension or stiffness, and as in the case of magnitudes B and C (Figs. 9B and 10B). Thus, H must have a molecular origin stemming from the activation mechanism, which is common to all magnitude-related parameters (H , B , C , Y_{∞} , and tension). This situation is quite different from that of fast twitch skeletal muscle fibers, in which H is a small constant (Kawai and Brandt 1980) and may have little meaning.

Magnitude H is a low-frequency component, and it likely includes Process A observed in fast twitch skeletal fibers (Kawai and Brandt 1980). While Process A is absent in experiments with cardiac preparations performed at $\leq 25 \text{ }^\circ\text{C}$, Process A emerges at higher temperatures ($\geq 30 \text{ }^\circ\text{C}$) (Lu et al. 2006). It is possible that H includes the effect of Process A when this is not visible. Process A correlates well with the ATP hydrolysis rate (Wang and Kawai 2013); hence, it may represent Step 6 in Fig. 4 with the rate constant r_6 , which is the slowest step in the CB cycle (Kawai and Zhao 1993). Because force is generated at Step 4 before Pi release (Step 5), and Step 6 is slower than Steps 4 and 5, it is likely that work performance takes place at Step 6. Movement generation requires a transfer of momentum, which takes a substantial amount of time (Kawai and Zhao 1993).

Conclusions

In conclusion, our studies demonstrate the usefulness of flash-frozen and cryo-sectioned cardiac muscle preparations and that we obtained excellent kinetic data with many meaningful insights into the molecular mechanisms of contraction. Furthermore, our studies demonstrate that Process C represents CBs undergoing detachment (Step 2), that Process B represents CBs performing force generation (Step 4), and that magnitude H represents CBs performing work (Step 6). The magnitude parameters (C , B , H) are primarily related with CB numbers in each state, hence flux (transition) between states. Their levels are activated by Ca^{2+} in a cooperative manner resulting in a large Hill

coefficient of 4–5. The effect of Ca^{2+} on the rate constant of the force generation step can be approximated by a second order reaction (Eq. 9).

Acknowledgements We would like to thank Professor Li Wang of Soochow University, China, for her enthusiastic help and moral support of this project and for sending JX to Iowa to carry out experiments reported in this paper. JY and JX were supported by the Research Start-up Fund of Jining Medical University (Reference: 600791001, JY). Chemicals, supplies, and the maintenance of lab equipment were provided by MK. The work done at the University of Illinois at Chicago was supported by grants from the National Institutes of Health (HL127691 and HL138007 to JJ). We also would like to thank Ms. Heather A. Widmayer with the University of Iowa Scientific Editing and Research Communication Core for English language editing.

Author contributions JX performed experiments, initial data analysis, and editing of the manuscript. HF prepared flash-frozen and cryo-sectioned papillary muscle preparations and bright field microscopy. JJ supervised muscle preparations and editing of the manuscript. JY initially financed the project, and edited the manuscript. MK planned experiments, wrote experimental and analysis computer programs, analyzed the data, drafted and edited the manuscript, and financed the project.

Funding This work is supported by the Research Start-up Fund of Jining Medical University (Grant No. 600791001), Office of Extramural Research, National Institutes of Health (Grant Nos. HL127691 and HL138007 to JPJ).

Data availability These are provided on request to Masataka-Kawai@uiowa.edu

Declarations

Conflict of interest There are no conflicts of interest among the authors involved.

References

- Abbott RH, Steiger GJ (1977) Temperature and amplitude dependence of tension transients in glycerinated skeletal and insect fibrillar muscle. *J Physiol* 266:13–42
- Bai F, Caster HM, Rubenstein PA, Dawson JF, Kawai M (2014) Using baculovirus/insect cell expressed recombinant actin to study the molecular pathogenesis of HCM caused by actin mutation A331P. *J Mol Cell Cardiol* 74C:64–75
- Bartoo ML, Popov VI, Fearn LA, Pollack GH (1993) Active tension generation in isolated skeletal myofibrils. *J Muscle Res Cell Motil* 14:498–510
- Colomo F, Piroddi N, Poggesi C, te Kronnie G, Tesi C (1997) Active and passive forces of isolated myofibrils from cardiac and fast skeletal muscle of the frog. *J Physiol* 500(Pt 2):535–548
- Dantzig J, Goldman Y, Millar NC, Laktis J, Homsher E (1992) Reversal of the cross-bridge force-generating transition by the photogeneration of phosphate in rabbit psoas muscle fibers. *J Physiol* 451:247–278
- Feng HZ, Jin JP (2020) High efficiency preparation of skinned mouse cardiac muscle strips from cryosections for contractility studies. *Exp Physiol* 105:1869–1881
- Ford LE, Huxley AF, Simmons RM (1977) Tension responses to sudden length change in stimulated frog muscle fibres near slack length. *J Physiol* 269:441–515
- Fortune NS, Geeves MA, Ranatunga KW (1991) Tension responses to rapid pressure release in glycerinated rabbit muscle fibers. *Proc Natl Acad Sci USA* 88:7323–7327
- Gordon AM, Huxley AF, Julian FJ (1966) The variation in isometric tension with sarcomere length in vertebrate muscle fibres. *J Physiol* 184:170–192
- Gutfreund H (1995) Kinetics for life sciences: receptors, transmitters and chatalysts. Cambridge University Press
- Harris DE, Warshaw DM (1993) Smooth and skeletal muscle actin are mechanically indistinguishable in the in vitro motility assay. *Circ Res* 72:219–224
- Heinl P, Kuhn HJ, Ruegg JC (1974) Tension responses to quick length changes of glycerinated skeletal muscle fibres from the frog and tortoise. *J Physiol* 237:243–258
- Hellam DC, Podolsky RJ (1969) Force measurements in skinned muscle fibres. *J Physiol* 200:807–819
- Hibberd MG, Dantzig JA, Trentham DR, Goldman YE (1985) Phosphate release and force generation in skeletal muscle fibers. *Science* 228:1317–1319
- Hill AV (1910) The possible effects of the aggregation of the molecules of haemoglobin on its dissociation curves. *J Physiol* 40(Suppl):4–7
- Hill AV (1938) The heat of shortening and the dynamic constants of muscle. *Proc Roy Soc (b)* 126:136–195
- Hill AV (1953) The mechanics of active muscle. *Proc R Soc Lond B Biol Sci* 141:104–117
- Huxley AF (1974) Muscular contraction. *J Physiol* 243:1–43
- Huxley AF, Simmons RM (1971) Proposed mechanism of force generation in striated muscle. *Nature* 233:533–538
- Jalal N, Zidi M (2018) Effect of cryopreservation at -80°C on visco-hyperelastic properties of skeletal muscle tissue. *J Mech Behav Biomed Mater* 77:572–577
- Julian FJ (1969) Activation in a skeletal muscle contraction model with a modification for insect fibrillar muscle. *Biophys J* 9:547–570
- Kawai M, Brandt PW (1980) Sinusoidal analysis: a high resolution method for correlating biochemical reactions with physiological processes in activated skeletal muscles of rabbit, frog and crayfish. *J Muscle Res Cell Mot* 1:279–303
- Kawai M, Halvorson H (1989) Role of MgATP and MgADP in the crossbridge kinetics in chemically skinned rabbit psoas fibers. Study of a fast exponential process C. *Biophys J* 55:595–603
- Kawai M, Halvorson HR (1991) Two step mechanism of phosphate release and the mechanism of force generation in chemically skinned fibers of rabbit psoas. *Biophys J* 59:329–342
- Kawai M, Zhao Y (1993) Cross-bridge scheme and force per cross-bridge state in skinned rabbit psoas muscle fibers. *Biophys J* 65:638–651
- Kawai M, Brandt P, Orentlicher M (1977) Dependence of energy transduction in intact skeletal muscles on the time in tension. *Biophys J* 18:161–172
- Kawai M, Saeki Y, Zhao Y (1993) Cross-bridge scheme and the kinetic constants of elementary steps deduced from chemically skinned papillary and trabecular muscles of the ferret. *Circ Res* 73:35–50
- Kawai M, Stehle R, Pfitzer G, Iorga B (2021) Phosphate has dual roles in cross-bridge kinetics in rabbit psoas single myofibrils. *J Gen Physiol*. <https://doi.org/10.1085/jgp.202012755>
- Kushmerick MJ, Moerland TS, Wiseman RW (1992) Mammalian skeletal muscle fibers distinguished by contents of phosphocreatine, ATP, and Pi. *Proc Natl Acad Sci USA* 89:7521–7525
- Lu X, Tobacman LS, Kawai M (2003) Effects of tropomyosin internal deletion Delta23Tm on isometric tension and the cross-bridge kinetics in bovine myocardium. *J Physiol* 553:457–471
- Lu X, Bryant MK, Bryan KE, Rubenstein PA, Kawai M (2005) Role of the N-terminal negative charges of actin in force generation

- and cross-bridge kinetics in reconstituted bovine cardiac muscle fibres. *J Physiol* 564:65–82
- Lu X, Tobacman LS, Kawai M (2006) Temperature-dependence of isometric tension and cross-bridge kinetics of cardiac muscle fibers reconstituted with a tropomyosin internal deletion mutant. *Biophys J* 91:4230–4240
- Lu X, Heeley DH, Smillie LB, Kawai M (2010) The role of tropomyosin isoforms and phosphorylation in force generation in thin-filament reconstituted bovine cardiac muscle fibres. *J Muscle Res Cell Motil* 31:93–109
- Pinzauti F, Pertici I, Reconditi M, Narayanan T, Stienen GJM, Piazzesi G, Lombardi V, Linari M, Caremani M (2018) The force and stiffness of myosin motors in the isometric twitch of a cardiac trabecula and the effect of the extracellular calcium concentration. *J Physiol* 596:2581–2596
- Piroddi N, Belus A, Scellini B, Tesi C, Giunti G, Cerbai E, Mugelli A, Poggesi C (2007) Tension generation and relaxation in single myofibrils from human atrial and ventricular myocardium. *Pflugers Arch* 454:63–73
- Podolsky RJ (1960) Kinetics of muscular contraction: the approach to the steady state. *Nature* 188:666–668
- Pringle JW (1967) The contractile mechanism of insect fibrillar muscle. *Prog Biophys Mol Biol* 17:1–60
- Rassier DE, Herzog W, Pollack GH (2003) Dynamics of individual sarcomeres during and after stretch in activated single myofibrils. *Proc Biol Sci* 270:1735–1740
- Reuben JP, Brandt PW, Berman M, Grundfest H (1971) Regulation of tension in the skinned crayfish muscle fiber. I. Contraction and relaxation in the absence of Ca (pCa is greater than 9). *J Gen Physiol* 57:385–407
- Ruegg JC, Tregear RT (1966) Mechanical factors affecting the ATPase activity of glycerol-extracted insect fibrillar flight muscle. *Proc R Soc Lond B Biol Sci* 165:497–512
- Shibata T, Hunter WC, Sagawa K (1987) Dynamic stiffness of barium-contracted cardiac muscles with different speeds of contraction. *Circ Res* 60:770–779
- Stehle R, Kruger M, Pfitzer G (2002) Force kinetics and individual sarcomere dynamics in cardiac myofibrils after rapid ca(2+) changes. *Biophys J* 83:2152–2161
- Sugi H, Gomi S (1984) Cinematographic studies on the A-band length changes during Ca-activated contraction in horseshoe crab muscle myofibrils. *Adv Exp Med Biol* 170:107–118
- Tesi C, Colomo F, Nencini S, Pirodi N, Poggesi C (2000) The effect of inorganic phosphate on force generation in single myofibrils from rabbit skeletal muscle. *Biophys J* 78:3081–3092
- Walker JW, Lu Z, Moss R (1992) Effects of Ca²⁺ on the kinetics of phosphate release in skeletal muscle. *J Biol Chem* 267:2459–2466
- Wang G, Kawai M (1997) Force generation and phosphate release steps in skinned rabbit soleus slow-twitch muscle fibers. *Biophys J* 73:878–894
- Wang L, Kawai M (2013) A re-interpretation of the rate of tension redevelopment (k_{TR}) in active muscle. *J Muscle Res Cell Motil* 34:407–415
- Wang L, Muthu P, Szczesna-Cordary D, Kawai M (2013a) Characterizations of myosin essential light chain's N-terminal truncation mutant Delta43 in transgenic mouse papillary muscles by using tension transients in response to sinusoidal length alterations. *J Muscle Res Cell Motil* 34:93–105
- Wang L, Muthu P, Szczesna-Cordary D, Kawai M (2013b) Diversity and similarity of motor function and cross-bridge kinetics in papillary muscles of transgenic mice carrying myosin regulatory light chain mutations D166V and R58Q. *J Mol Cell Cardiol* 62:153–163
- Wang L, Sadayappan S, Kawai M (2014) Cardiac myosin binding protein C phosphorylation affects cross-bridge cycle's elementary steps in a site-specific manner. *PLoS ONE* 0113417:1–21
- Wannenburg T, Heijne GH, Geerdink JH, Van-Den-Dool HW, Janssen PM, DeTombe PP (2000) Cross-bridge kinetics in rat myocardium: effect of sarcomere length and calcium activation. *Am J Physiol* 279:H779–H790
- Webb M, del Jackson R, Stewart TJ, Dugan SP, Carter MS, Cremonese CR, Baker JE (2013) The myosin duty ratio tunes the calcium sensitivity and cooperative activation of the thin filament. *Biochemistry* 52:6437–6444
- White DC, Thorson J (1972) Phosphate starvation and the nonlinear dynamics of insect fibrillar flight muscle. *J Gen Physiol* 60:307–336
- Woody MS, Winkelmann DA, Capitanio M, Ostap EM, Goldman YE (2019) Single molecule mechanics resolves the earliest events in force generation by cardiac myosin. *Elife*. 8.
- Xi J, Ye Y, Mokadem M, Yuan J, Kawai M (2022) The effect of gender and obesity in modulating cross-bridge function in cardiac muscle fibers. *J Muscle Res Cell Motil* 43:157–172
- Zhang J, Wang L, Kazmierczak K, Yun H, Szczesna-Cordary D, Kawai M (2021) Hypertrophic cardiomyopathy associated E22K mutation in myosin regulatory light chain decreases calcium-activated tension and stiffness and reduces myofilament Ca(2+) sensitivity. *Febs J* 288:4596–4613
- Zhao Y, Kawai M (1996) Inotropic agent EMD 53998 weakens nucleotide and phosphate binding to cross bridges in porcine myocardium. *Am J Physiol* 271:H1394–H1406

Publisher's Note Springer Nature remains neutral with regard to jurisdictional claims in published maps and institutional affiliations.

Springer Nature or its licensor (e.g. a society or other partner) holds exclusive rights to this article under a publishing agreement with the author(s) or other rightsholder(s); author self-archiving of the accepted manuscript version of this article is solely governed by the terms of such publishing agreement and applicable law.